UC Berkeley
UC Berkeley Previously Published Works

Title
Exploring the Ion Solvation Environments in Solid-State Polymer Electrolytes through Free-Energy Sampling

Permalink
https://escholarship.org/uc/item/2488g43t

Journal
Macromolecules, 54(18)

ISSN
0024-9297

Authors
Sundararaman, Siddharth
Halat, David M
Choo, Youngwoo
et al.

Publication Date
2021-09-28

DOI
10.1021/acs.macromol.1c01417

Peer reviewed

Macromolecules

Article

Exploring the Ion Solvation Environments in Solid-State Polymer Electrolytes through Free-Energy Sampling

Siddharth Sundararaman,* David M. Halat, Youngwoo Choo, Rachel L. Snyder, Brooks A. Abel, Geoffrey W. Coates, Jeffrey A. Reimer, Nitash P. Balsara, and David Prendergast

Cite This: https://doi.org/10.1021/acs.macromol.1c01417
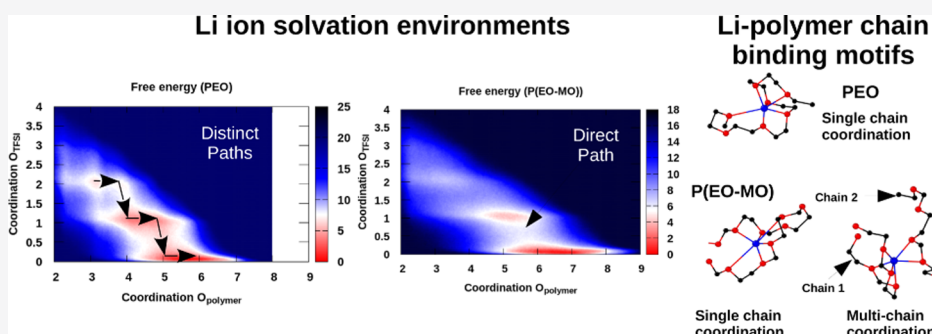
Read Online

ACCESS | 📊 Metrics & More | 📑 Article Recommendations | 🔲 Supporting Information

ABSTRACT: The success of polyethylene oxide (PEO) in solid-state polymer electrolytes for lithium-ion batteries is well established. Recently, in order to understand this success and to explore possible alternatives, we studied polyacetal electrolytes to deepen the understanding of the effect of the local chemical structure on ion transport. Advanced molecular dynamics techniques using newly developed, tailored interaction potentials have helped elucidate the various coordination environments of ions in these systems. In particular, the competition between cation–anion pairing and coordination by the polymer has been explored using free-energy sampling (metadynamics). At equivalent reduced temperatures, with respect to the polymer-specific glass-transition temperature, two-dimensional free-energy plots reveal the existence of multiple coordination environments for the lithium (Li) ions in these systems and their relative stabilities. Furthermore, we observe that the Li-ion movement in PEO follows a serial, stepwise pathway when moving from one coordination state to another, whereas this happens in a more continuous and concerted fashion in a polyacetal such as poly(1,3-dioxalane) [P(EO-MO)]. The implication is that interconversion between coordination states of the Li ions may be easier in P(EO-MO). However, the overarching observation from our free-energy analysis is that Li-ion coordination is dominated by the polymer (in either case) and contact-ion pairs are rare. We rationalize the observed higher increase in glass-transition temperature (T_g) with salt loading in polyacetals as due to intermolecular Li-ion coordination involving multiple polymer chains, rather than just one chain for PEO-based electrolytes. This interchain coupling in the polyacetals, resulting in the higher T_g, works against any gains due to variations in Li-ion coordination that might enhance transport processes over PEO. Further research is required to overcome the interdependence between local coordination and macroscopic properties to compete with PEO electrolytes at the same absolute working temperature.

■ INTRODUCTION

Lithium-ion batteries are high-energy-density power sources that find uses in the automobile industry for electric cars and various portable devices like smartphones and laptops.[1,2] There are strong motivations for developing solid-state electrolytes, with solid polymer electrolytes (SPEs) being prime candidates, since they have strong mechanical stability and avoid safety concerns associated with the combination of flammable liquid electrolytes and cell shorting due to lithium dendrite growth in the current technology.[3−9] Since the early work of Wright[10,11] and Armand,[12] poly(ethylene oxide) (PEO) has been studied extensively and has remained one of the more promising SPEs.[6,13,14] Polymer electrolytes usually behave as hosts for the ions in the system, with the ions having the ability to move through the free volume of the polymers assisted by the segmental motion, with reasonable conductivity possible above the glass-transition temperature.[6] Therefore, effective dissolution of the cations and a low glass-transition temperature are key to good ionic properties in these systems.[13] Unfortunately, slow ionic conductivities and low transference numbers in

SPEs at battery working temperatures have significantly hindered their performance for practical applications.[6,13−18]

Standard molecular dynamics (MD) protocols have been used extensively to explore the ion coordination environments and try to understand the transport mechanism in PEO/lithium bis(trifluoromethanesulfonyl)imide (LiTFSI) systems.[19−28] Borodin and Smith[21] used a quantum chemistry-based many-body polarizable force field to look at the local ion coordination environment, ion aggregation, and various contributions to cation transport. They found in their simulations that Li-ion motion is a combination of motion along the polymer chains, along with the segmental motion of PEO, and ion hopping from one segment to another at different timescales. Motivated by experimental findings,[29] Diddens and Heuer confirmed that at lower salt concentrations, all Li ions are coordinated by PEO chains and that the improved Li-ion transport with addition of ionic liquids was due to the plasticizing effect of the ionic liquid molecules.[22] Recently, Molinari and co-workers[24] showed that asymmetrical negatively charged clusters at high LiTFSI concentrations are a possible reason for experimental negative transference numbers. Standard MD protocols are however plagued by drawbacks of system size effects, starting configuration dependence, and limited sampling as compared to residence times in coordination environments that can affect the accuracy of the various ensemble averages calculated in spite of the long times that are usually used in these simulations. Recent work by Baskin and Prendergast[30,31] illustrated the use of free-energy sampling methods like umbrella sampling[32,33] and metadynamics[34,35] in the framework of both classical and ab initio MD to overcome some of these deficiencies and gain more rigorous insight into ion solvation environments.

In our previous work,[36,37] the design strategy that was employed was to maintain a high oxygen to carbon ratio in the backbone of the polymer to provide sufficient well-connected solvation sites for the Li cation by incorporating methylene oxide (O−CH$_2$ or MO) repeat units into the polymer backbone along with ethylene oxide (O−CH$_2$−CH$_2$ or EO). A series of such polyacetals with varying ratios of EO and MO in the repeat units, P(nEO-mMO), were synthesized[36] and systematically studied electrochemically[37] and through pulsed field gradient nuclear magnetic resonance spectroscopy measurements and MD simulations.[36] The polymers studied previously were P(EO-2MO), P(EO-MO), P(2EO-MO), P(3EO-MO), and P(4EO-MO) compared to PEO with LiTFSI salt. Polyacetal−LiTFSI SPEs were studied at similar reduced temperatures ($T − T_g$) as the glass-transition temperatures in the presence of LiTFSI varied significantly. It was observed that at a given reduced temperature, the cation self-diffusion coefficient was higher in each polyacetal derivative as compared to PEO. It was also observed that P(EO-MO) and P(EO-2MO) exhibit significantly lower anion self-diffusion coefficients as compared to the polyacetals in the series. Preliminary MD simulations revealed that the MO repeat units containing polymers (i.e., polyacetals) have additional ether oxygens close to the cation coordination environment in a second coordination shell, which distort the primary coordination environment and possibly improve Li-ion transport at a given reduced temperature in these systems.

In the present work, we use MD simulations and free-energy sampling (metadynamics) to gather further atomic level insight into the different coordination environments that exist in these systems, their relative stabilities, and how they might affect transport mechanisms. Our goal is to understand the underlying structural differences in the lithium coordination environments in these poly(ether-acetal) systems and how interchangeable they are. For simplicity, we compare PEO to P(EO-MO), the most efficacious polymer of the polyacetals studied previously.[37] We observe from metadynamics simulations the existence of multiple stable coordination environments with differing numbers of coordinating oxygen atoms from the polymer and TFSI. The importance of running advanced free-energy calculations as compared to a regular MD protocol is most notable upon examination of the relative stabilities of various coordination environments, which might easily form irreversibly during tractable MD simulations, thereby overestimating their statistical significance. Furthermore, PEO exhibits a serial, stepwise minimum free-energy pathway to convert from one coordination state to another, while P(EO-MO) has a more direct, continuous pathway with the transition occurring in a more concerted fashion. However, we know that the polyacetals experience a larger increase in T_g upon addition of LiTFSI salt, which works against any enhanced transport mechanisms at the same absolute temperature. Our simulations indicate that this is due to enhanced interchain connectivity through Li-ion coordination in the polyacetals. Overall, these insights provide a fundamental understanding of the structural differences between local coordination of Li ions in both systems and indicate that reducing the T_g increase upon salt loading should be key to defining new chemistries for SPEs and improving performance for Li-ion battery applications.

■ METHODS

The Methods section is divided into three parts. In the first part, we describe the MD protocol that we use to prepare the polymer systems with ions at various concentrations. In the second part, we delve into the functional form of the force field and the methods used to optimize the existing generalized AMBER force field (GAFF) interaction potential[38] to predict the angles, bonds, dihedrals, and bulk properties, such as density, more reliably over a wide range of compositions. Finally, we elaborate on the free-energy calculations performed using these newly optimized potentials to reveal the prevalent coordination environments of the ions and to explore the mechanism of contact-ion-pair formation.

MD Protocol. MD simulations were performed using the large-scale atomic/molecular massively parallel simulator (LAMMPS) code[39] using an interaction potential with the GAFF[38] functional form

$$E_{\text{tot}} = \sum_{\text{bonds}} K_r(r - r_0)^2 + \sum_{\text{angles}} K_\theta(\theta - \theta_0)^2$$
$$+ \sum_{\text{dihedrals}} K_\phi[1 + d\cos(n\phi)]$$
$$+ \sum_{i<j} \left(4\epsilon_{ij}\left[\frac{\sigma_{ij}^{12}}{r_{ij}^{12}} - \frac{\sigma_{ij}^{6}}{r_{ij}^{6}} \right] + \frac{q_i q_j}{4\pi\epsilon_0 r_{ij}} \right) \tag{1}$$

where K_r, K_θ, and K_ϕ are force constants; r_0, θ_0, and ϕ_0 are the equilibrium bond length, bond angle, and dihedral angle, respectively; n is the multiplicity; the σ_{ij} and ϵ_{ij} parameters characterize a Lennard-Jones (LJ) non-bonded interaction; and q_i is the partial charge on the atoms. The total energy E_{tot} is hence expressed as a summation of harmonic bond, angle, and dihedral terms that are primarily intrachain in nature and LJ and electrostatic interactions that largely determine interchain interactions (although they are relevant if the polymer chain is highly curved or forms loops). The partial charges were calculated using the restrained electrostatic potential (RESP) model[40] after ab initio optimization of isolated molecules with the B3LYP hybrid density functional and the 6-311++gss basis set using

162 TeraChem.[41−43] The charges on the ions were scaled by 0.8 based on
163 ab initio results and suggestions from the previous literature[44,45] to
164 emulate polarization effects. Geometric mixing rules were used for
165 unlike LJ parameters (σ_{ij}, ϵ_{ij}). Intramolecular pairwise LJ and
166 coulombic interactions separated by one and two bonds were set to
167 0, while those separated by three were set to 0.8 and 0.5, respectively.
168 The short-range cutoff was set to 13 Å, while the electrostatic
169 interactions were cut off at 14 Å. The time step used for all our MD
170 simulations was 1 fs unless otherwise specified.

171 A multi-step annealing protocol was used to create the MD
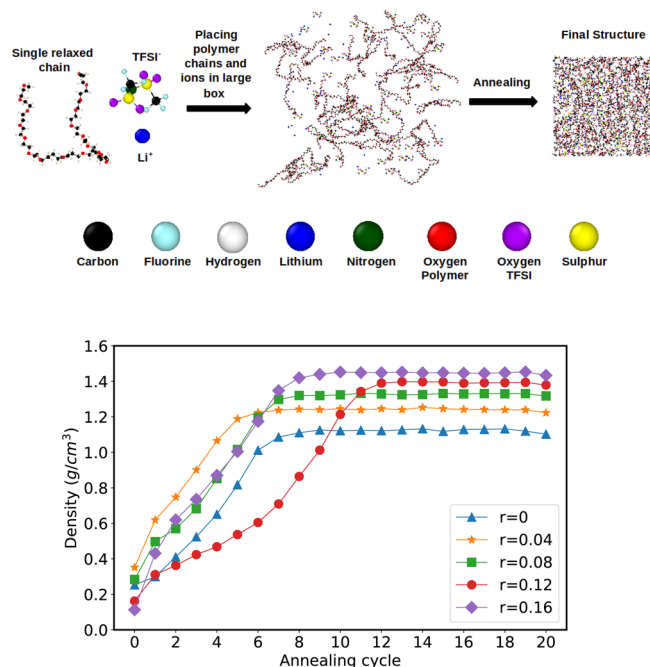172 structures used in this work (see the top panel of Figure 1). A single

f1

Figure 1. Top: Schematic for ion−polymer system preparation; bottom: saturation of density with annealing cycles.

173 chain of the polymer with a chain length of 15−20 monomer units
174 was first created and relaxed in the *NVT* ensemble [where *NVT*
175 implies a constant number of particles (N), volume (V), and
176 temperature (T)] at 300 K. A total of 30 such relaxed chains were
177 placed in a large box at a very low density (0.1−0.25 g/cm³) to avoid
178 any overlap, and the correct amount of Li and TFSI ions for the
179 specific composition were randomly distributed. Salt concentrations
180 studied in this work ranged from $r = 0$ to 0.16, where $r = [\text{Li}]/[\text{O}]$
181 (the ratio of Li ions to polymer oxygens), with the upper bound
182 defined by involvement of all available O atoms in Li-ion
183 coordination, assuming an average of 6 coordinating O atoms per
184 Li ion. Each annealing cycle consisted of first heating the system from
185 300 to 900 K in steps of 60 K, relaxing at each step for 20 ps at a
186 nominal heating rate of 3 K/ps, relaxing the system for 100 ps at that
187 temperature and slowly cooling down the system again in steps of 60
188 K at a nominal cooling rate of 3 K/ps in the *NVT* ensemble, followed
189 by a room-temperature relaxation in the *NPT* ensemble [where *NPT*
190 implies a constant number of particles (N), pressure (P), and
191 temperature (T)] at 300 K at atmospheric pressure (1 bar) for 50 ps,
192 allowing for the density to change. The variation of density with each
193 annealing cycle is shown in the bottom panel of Figure 1. Based on
194 these data, we chose to perform 20 annealing cycles for each system to
195 ensure that the system has reached an equilibrium density. The
196 resulting samples were then heated to various temperatures and
197 relaxed for 50−100 ns in the *NVT* ensemble for further structural
198 analysis.

199 **Potential Optimization.** As stated above, the first three terms in
200 eq 1 that define polymer interactions are intrachain in nature, largely
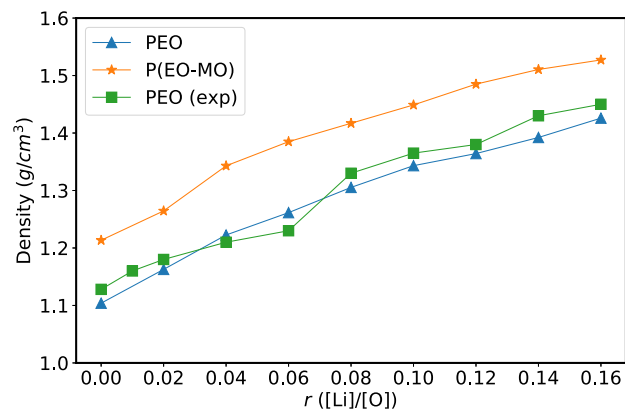201 determining the bonds, angles, and dihedrals, respectively, while the

202 interchain interactions are determined by LJ and electrostatic
203 interactions. Hence, we can reasonably separate the optimization of
204 the intrachain parameters to predict the correct bonds, angles, and
205 dihedrals, while holding the charge and the LJ parameters fixed, and
206 modify the latter to optimize bulk properties, such as mass density.

207 Optimizing the existing GAFF interaction potential[38] first required
208 a reliable set of reference data for bonds, angles, and dihedrals which
209 were produced by relaxing various isolated structures of the monomer
210 or dimer using density functional theory, as described in the previous
211 section. As mentioned previously, the partial charges for the
212 optimization were calculated using the RESP model,[40] with the
213 charges on the ions scaled by 0.8 based on ab initio results and
214 suggestions from the previous literature[44,45] to emulate polarization
215 effects. Figure 2 shows the density predicted by the new optimized

f2

Figure 2. Density predicted by the newly optimized potential for PEO and P(EO-MO) at varying salt loadings compared to available experimental results for PEO.[46]

216 potential for two systems of interest, PEO and P(EO-MO), compared
217 with experimental data for PEO.[46] It is observed that our new
218 potential performs well in predicting the measured density of PEO for
219 a wide salt concentration range (see Tables S1−S4 for details).

220 Furthermore, when we tested the interaction potentials for
221 oligomers of different lengths, we observed that the original
222 (unoptimized) GAFF interaction potential was unable to predict
223 the densities correctly over a range of lengths (see Figure S1). Our
224 optimized potential performed well for the longer oligomers
225 (approximating the polymer) but was not able to predict the density
226 correctly at shorter lengths (approximating a molecular liquid). To
227 address this issue, we modified the LJ interaction for terminal carbons
228 in each chain to be slightly more repulsive (by increasing σ by a factor
229 of 1.25 and reducing ϵ by the same factor)—terminal interactions
230 necessarily begin to dominate for shorter oligomers. With this
231 modification (see Table S5 for modified parameters), we see that the
232 previously observed accuracy in predicting the density of long
233 oligomers (>8 repeat units) remains unaffected, but now, we can also
234 reproduce the density for shorter chain lengths. We include this detail
235 for future work. However, the metadynamics simulations for longer
236 oligomers reported below were performed using our first density-
237 optimized potential and were not repeated to include this
238 modification of termini repulsion. Smaller-scale simulations for
239 these approximations to polymer systems showed no discernible
240 differences with either potential.

241 **Metadynamics.** Polymer conformations produced using the
242 aforementioned simulated annealing protocol were used as initial
243 configurations to perform free-energy calculations using the
244 metadynamics approach. It is important to note that the T_g values
245 predicted by our potential are relatively high as compared to
246 experimentally determined T_g values and, hence, for similar
247 phenomenological results, we studied these systems at similar effective
248 temperatures as compared to experiments. The PEO and P(EO-MO)
249 electrolytes studied here had the same salt concentration, $r = 0.08$,
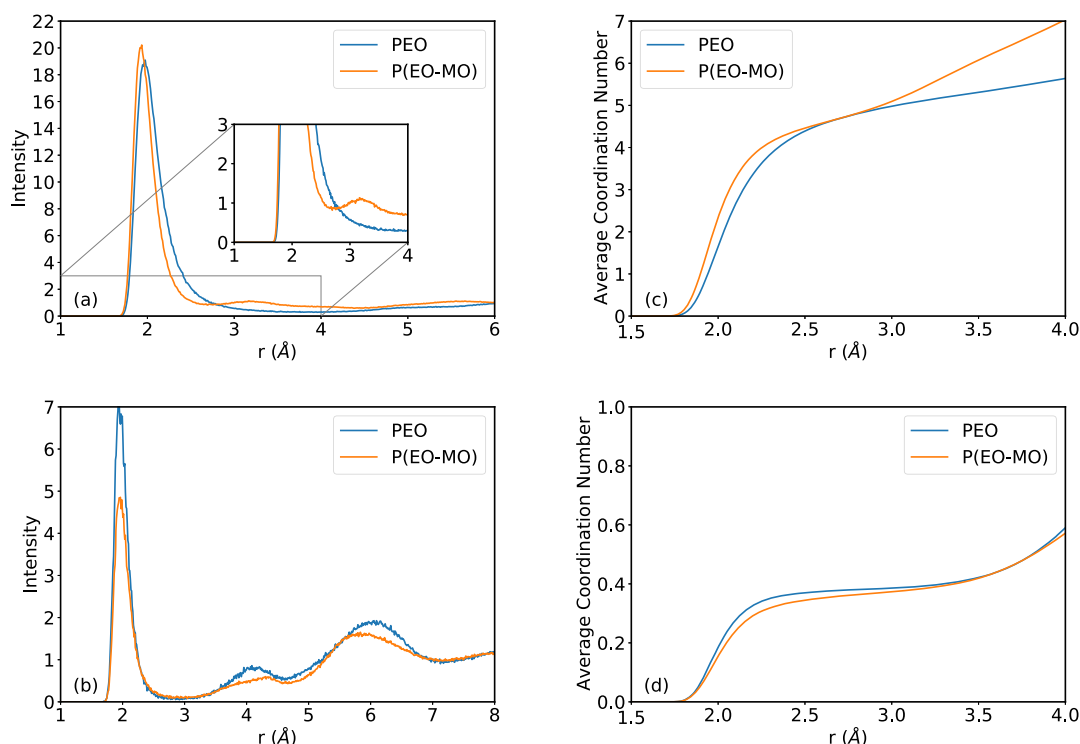
Figure 3. Radial distribution function of the Li ions with respect to the oxygen atoms from the (a) polymer and (b) TFSI and the corresponding CNs (c,d), respectively.
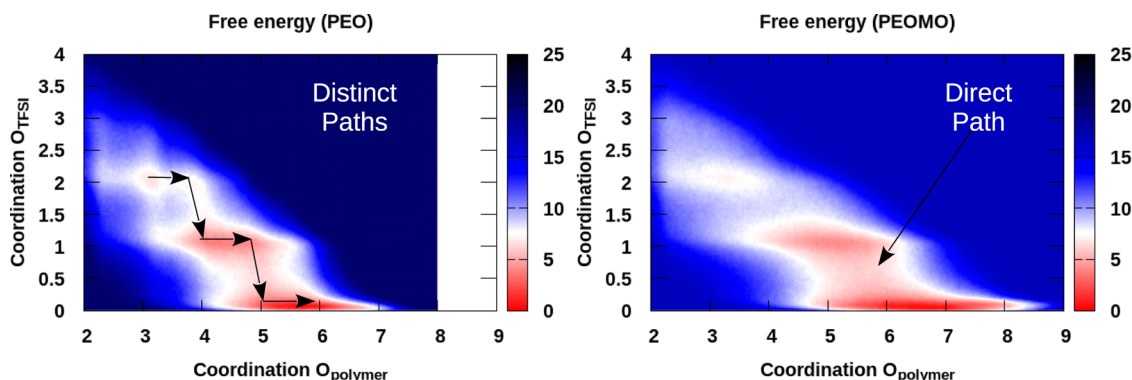

Figure 4. Pathways: 2D free-energy analysis of solvation of the Li cation and TFSI anion in PEO and P(EO-MO). Coordination with respect to oxygens of ether/acetyl and oxygens of TFSI anions are used as collective variables. Serial process: PEO shows distinct stepwise pathways to move from one coordination state to another (arrows for guide show the polymer oxygen forming a bond in the first step and then the TFSI oxygen bond breaking in the second step). Concerted process: P(EO-MO) shows a more direct path that implies that bond breaking and forming happen in a more concerted way that allows for easier switching among cation coordinations.

and were held at effective temperatures ($T_{eff} = T - T_g$) of about 120 K, corresponding to absolute temperatures of 573 and 648 K, respectively. The first collective variable used in this analysis was the coordination number (CN) of a Li ion with respect to oxygen atoms from the anion (TFSI). The other collective variable was the CN of a Li ion with respect to the oxygen atoms of the polymer. These collective variables together represent the enthalpy of solvation of the lithium ion in different coordination environments. The CN is calculated as follows:

$$CN(\text{type 1, type 2}) = \sum_{i \in \text{type1}} \sum_{j \in \text{type2}} \frac{1 - \left(\frac{|r_i - r_j|}{r_0}\right)^6}{1 - \left(\frac{|r_i - r_j|}{r_0}\right)^{12}} \quad (2)$$

where type 1 is a specific Li ion in our simulations, type 2 is either oxygen of the anion or oxygen of the polymer, and r_0 is the cutoff

distance defined for the two groups of atoms. This definition of CN[47] provides a continuous function, which is why we can have non-integral CNs in our simulations. The various parameters used for the metadynamics simulations such as height (H, kcal/mol) and width (W, unitless) of the Gaussian hills, frequency of hill addition (F, freq, steps), cutoff used for measuring the CN of the Li ion with the polymer and TFSI oxygen atoms ($r_0^{\text{Li}-\text{poly}}$ and $r_0^{\text{Li}-\text{TFSI}}$, Å), and the simulation time of the calculations (t, ns) are all listed in Table S6 for both the initial tests and the production runs.

These simulations are performed at a finite salt concentration, with a fixed number of Li ions in the simulation cell, but our analysis focuses on a single, randomly chosen Li ion. Therefore, we checked for independence of our results on the specific choice of the Li ion. Metadynamics simulations were performed based on using CNs centered around three different Li ions for each system with different starting coordination environments (see Table S7). Irrespective of the Li ion chosen or its initial coordination environment, the resulting
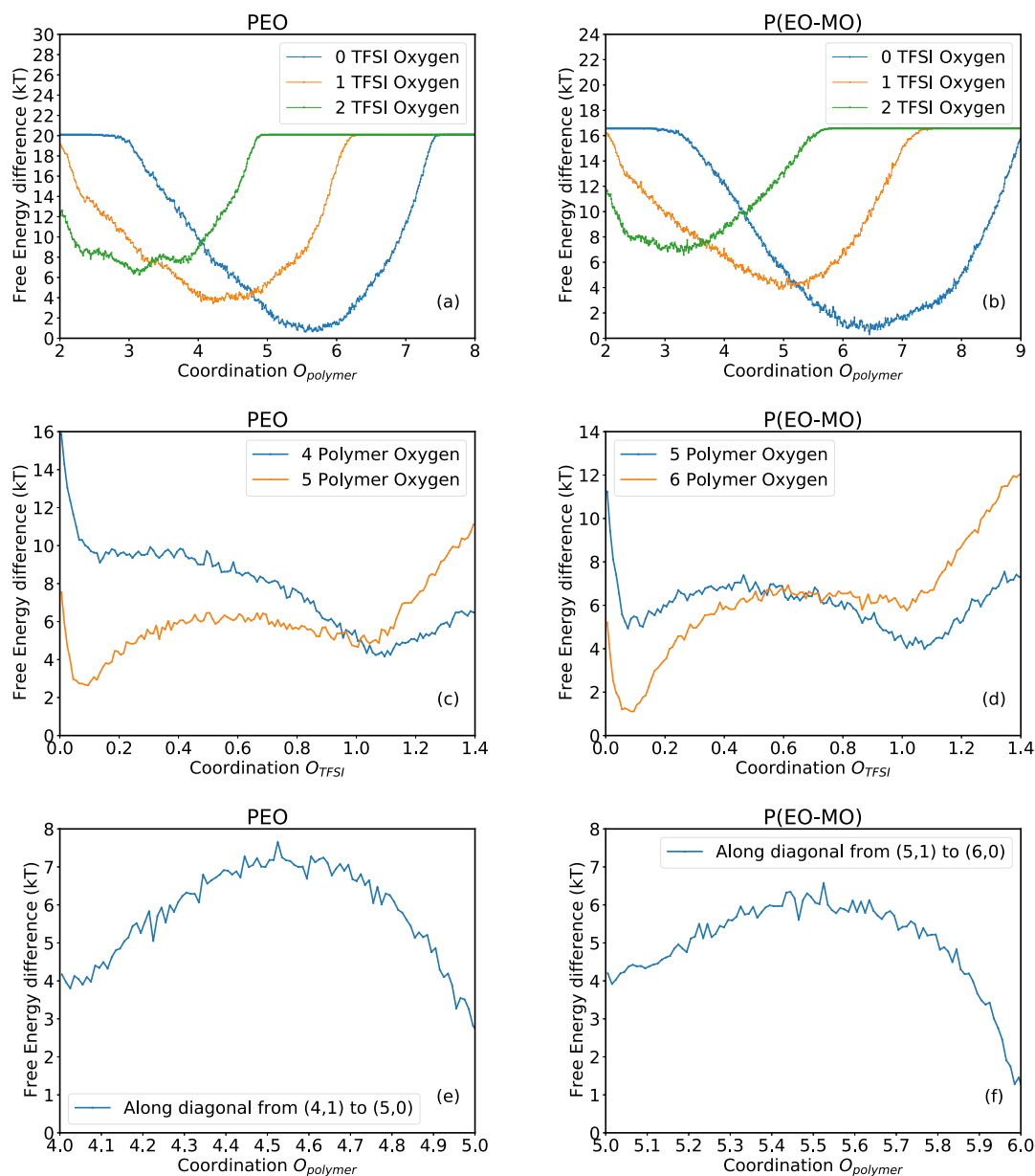
Figure 5. 1D cut of the free-energy curves at different numbers of oxygens from TFSI for (a) PEO and (b) P(EO-MO), at different numbers of oxygens from the polymer for (c) PEO and (d) P(EO-MO), and along a diagonal from (4,1) to (5,0) for (e) PEO and (5,1) to (6,0) for (f) P(EO-MO).

free-energy landscapes are practically identical (see Figure S2). Based on this sensitivity analysis, we continued running only one of the simulations for each system to conserve computational time.

■ RESULTS AND DISCUSSION

This section is divided into two parts: first, we investigated the local structural differences in the Li-ion coordination environments within PEO and P(EO-MO) and then performed free-energy calculations at the same effective temperature ($T_{eff} = T - T_g$) to reveal the relative stability of distinct ion coordinations and the energy barriers to their interconversion. Next, we delved into the effect of salt loading on T_g in the poly(ether-acetal) series to understand why each polymer derivative responds differently and how this affects the performance of SPEs for battery applications.

Understanding Coordination Environments. MD simulations using our optimized interaction potentials have

helped to reveal subtle differences in the Li-ion coordination environment in the poly(ether-acetals) series (see Figure 3a for radial distribution functions and Figure 3c for average CN with respect to polymer oxygen atoms). In our previous work,[36] we observed that polymers containing MO units exhibit a second oxygen coordination shell around the Li ion, which appears to distort the first coordination shell [see the second peak in the P(EO-MO) radial distribution function, between 3 and 4 Å, the inset of Figure 3a]. Our presumption is that this may create a more open cage structure around the Li ion that facilitates ion transport from one cage to another. The distorted Li-ion coordination environment may also assist in the formation of a lower coordination transition state while the Li ions move from one cage to another. We also see that Li ions in P(EO-MO) have a higher average CN (CN = 7) as compared to PEO (CN = 6), but the increased CN is limited to intermediate distances (3–4 Å).

Table 1. Probability of Finding a Li Ion in Different Coordination Environments in PEO

coordination state	energy (kT)	probability (metadynamics)	probability (regular MD protocol) 50 ns	probability (regular MD protocol) 100 ns
(2,2)	12.480	1.252×10^{-5}	0.0009	0.0016
(3,2)	6.941	0.003185	0.0071	0.0078
(4,2)	8.892	4.527×10^{-4}	0.0073	0.0056
(3,1)	9.717	1.984×10^{-4}	0.0074	0.0074
(4,1)	4.169	0.0510	0.0904	0.0914
(5,1)	5.530	0.0130	0.0639	0.0631
(6,1)	17.04	1.310×10^{-7}	0.0076	0.0072
(4,0)	9.907	1.641×10^{-4}	0.0200	0.0192
(5,0)	2.648	0.2330	0.2946	0.3022
(6,0)	1.550	0.6990	0.4612	0.4578
(7,0)	11.59	3.048×10^{-5}	0.0397	0.0368

Table 2. Probability of Finding a Li Ion in Different Coordination Environments in P(EO-MO)

coordination state	energy (kT)	probability (metadynamics)	probability (regular MD protocol) 50 ns	probability (regular MD protocol) 100 ns
(2,2)	11.80	1.266×10^{-5}	0.0025	0.0029
(3,2)	7.288	0.0012	0.0042	0.0044
(4,2)	8.701	2.807×10^{-4}	0.0033	0.0034
(3,1)	9.688	1.046×10^{-4}	0.0039	0.0043
(4,1)	6.334	0.0030	0.0466	0.0476
(5,1)	4.200	0.0253	0.0476	0.0483
(6,1)	6.699	0.0021	0.0129	0.0129
(5,0)	5.490	0.0070	0.2175	0.2205
(6,0)	1.110	0.5560	0.4206	0.4162
(7,0)	1.455	0.3940	0.2090	0.2078
(8,0)	4.986	0.0012	0.0319	0.0317

Our MD simulations indicate a reduced propensity for cation−anion pairs in P(EO-MO) versus PEO [see the reduced intensity in the first peak of the radial distribution function (see Figure 3b) and the overall reduction in average CN with respect to O atoms in TFSI (see Figure 3d)]. We rationalize this observation as due to the more negative partial charge on the MO oxygen atoms as compared to the oxygen atoms of EO moieties. In this sense, P(EO-MO) can compete more effectively than PEO against the TFSI anion for coordinating Li ions, thereby resulting in a lower number of ion pairs.

Free-energy calculations further elucidate the relative stabilities of the distinct Li−O coordination environments and the possible pathways to move between them (see Figure 4). Our results suggest that multiple Li-ion coordination environments coexist in both PEO and P(EO-MO), as evidenced by multiple deep minima.

In PEO, we observe that the deepest free-energy minimum is close to coordinations (5,0) and (6,0), that is, with 5−6 oxygen atoms from the polymer ($O_{polymer}$) and no oxygen atoms from the TFSI anion (O_{TFSI}). The second most stable coordination states are at (5,1) and (4,1), that is, with 1 O_{TFSI} and 4−5 $O_{polymer}$, and further less stable minima are found near (2,2), (3,2), (4,2), (3,1), (6,1), (4,0), and (7,0). Similarly in P(EO-MO), we observe that the deepest minimum is close to (6,0) and (7,0), that is, with no O_{TFSI} and 6−7 $O_{polymer}$. The second most stable coordination state is at (5,1), and further

less stable minima are found near (2,2), (3,2), (4,2), (3,1), (4,1), (6,1), (5,0), and (8,0).

Figure 5a,b shows horizontal one-dimensional (1D) free-energy cuts for PEO and PEOMO through the two-dimensional (2D) landscapes for various O_{TFSI}, Figure 5c,d shows similar vertical cuts for various $O_{polymer}$, and Figure 5e,f shows a cut along a diagonal from (4,1) to (5,0) for PEO and (5,1) to (6,0) for P(EO-MO).

Based on the free energies of each minimum, we calculated the approximate probability of a Li ion being in a given coordination state by using an approximate partition function. If ΔG_i is the relative free energy of a specific coordination environment, then the probability of finding a Li ion in that environment (p_i) is given by eq 3

$$p_i = \frac{e^{-\beta \Delta G_i}}{\sum_j e^{-\beta \Delta G_j}} \tag{3}$$

where $\beta = 1/k_B T$. The probability of finding Li ions in each of the distinct coordination environments considered is calculated based on this partition function and summarized in Table 1 for PEO and Table 2 for P(EO-MO). Direct comparison is provided based on MD sampling over 50 and 100 ns from regular (unbiased) trajectories in the NVT ensemble at the same temperature.

Our free-energy calculations show that the most likely Li-ion coordination environment involves 6 polymer oxygen atoms in both PEO and P(EO-MO), with no coordination to the oxygen atoms from the TFSI anion. The second most stable coordination state of the Li ion in both cases also excludes the anion, with a higher coordination state, (7,0), preferred in P(EO-MO) but the lower coordination state (5,0) preferred in PEO. In addition, P(EO-MO) exhibits a higher relative probability for the second coordination state versus PEO. We observe that the MD protocol and the free-energy calculations in both systems give the same order of relative stability for the various coordination environments. However, we see significant differences between the MD-sampled Li-ion coordination state probabilities and those estimated based on the relative free energies derived from metadynamics [see especially state (5,0) for P(EO-MO) in Table 2]. Overall, the low-probability coordination environments have higher populations in the MD trajectories, which we consider to be overestimates. This can be attributed to the relatively high residence times of certain ion coordination environments as compared to the total duration of the MD simulations of 50 ns and 100 ns in the regular MD protocol. It is also important to note that the probability of the various coordination states does not change significantly in the 50 ns between these two regular MD simulations. This would imply either that the regular MD protocol has equilibrated or the more likely scenario that it is stuck in a deep local minimum. Without foresight on the depth of the free-energy landscape, we cannot predict the convergence time. This further establishes the need for free-energy calculations, such as metadynamics, to avoid such pitfalls in regular MD protocols. Metadynamics has an inbuilt mechanism to iteratively add bias to the system to permit exploration of the various coordination environments in a reasonable amount of time. Furthermore, from Figure 4, we also confirm our previous hypothesis that the coordination environment in P(EO-MO) is more diffuse than in PEO as evidenced from the much wider minima in the free-energy curves.
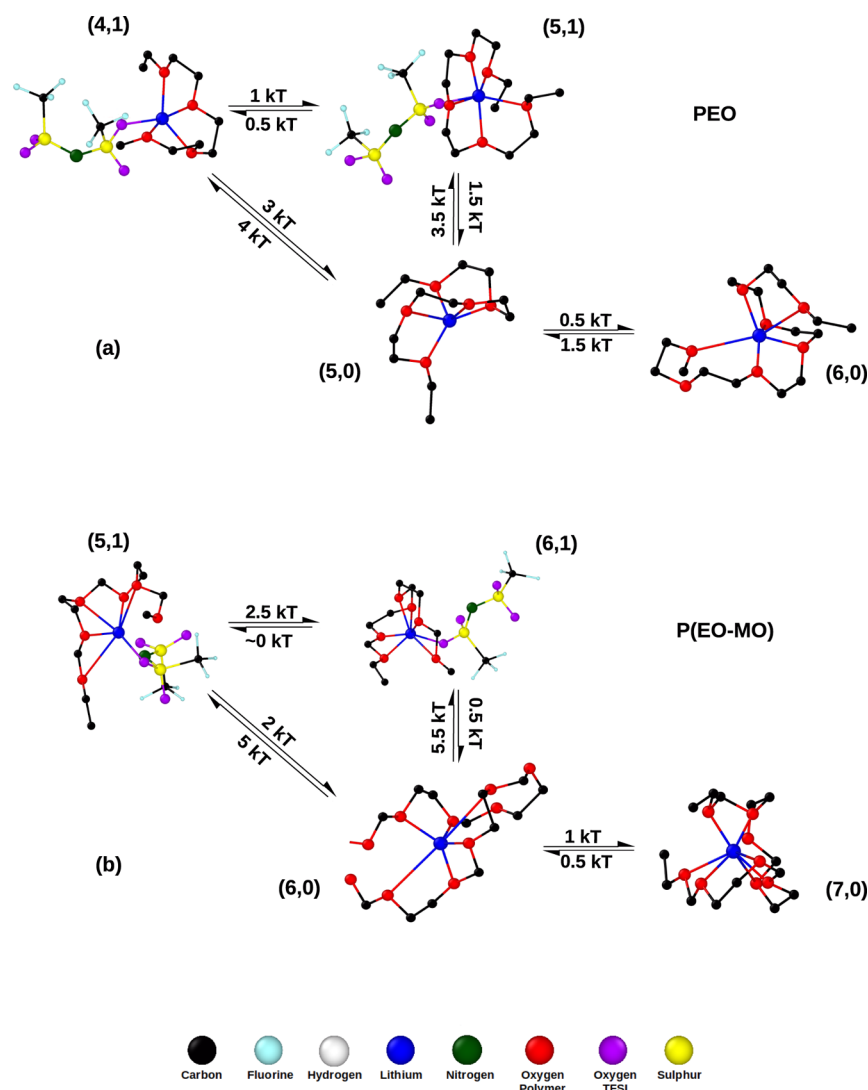
Figure 6. Representative snapshots of some of the coordination environments along with the energy barriers to transition from one state to another in (a) PEO at 573 K and (b) P(EO-MO) at 648 K.

Another important insight gained from these calculations are the minimum free-energy pathways between different coordination environments (see Figure 4). PEO exhibits a serial, stepwise minimum free-energy pathway of bond making and breaking to move from one coordination state to another (Figure 4). To go from the (4,1) state to the (5,0) state in PEO, the minimum energy pathway for the Li ion is to first form an additional bond with a polymer oxygen atom, that is, (4,1) to (5,1), which requires an activation energy of about $1kT$ (see Figure 5a), followed by breaking a TFSI oxygen bond, that is, (5,1) to (5,0), which requires an activation energy of about $1.5kT$ (see Figure 5c). To go directly from the (4,1) to (5,0) state, PEO would require an activation energy of about $3kT$ (see Figure 5e). The energy barriers for some of these transitions along with representative snapshots of coordination states are summarized in Figure 6a.

P(EO-MO), on the other hand, has a more direct free-energy minimum pathway with the bond breaking and forming happening in a more concerted fashion. To go from (5,1) to (6,0) in P(EO-MO), the minimum energy pathway is a diagonal connecting the two states with the TFSI oxygen bond breaking and polymer oxygen bond forming happening

simultaneously with an energy barrier of about $2kT$ (see Figure 5f). A stepwise pathway of first going from (5,1) to (6,1) would require overcoming an energy barrier of $2.5kT$ first (see Figure 5b), followed by another $0.5-1kT$ to move from (6,1) to (6,0) (see Figure 5d), which is energetically unfavorable. The energy barriers for some of these transitions along with representative snapshots of the coordination states are summarized in Figure 6b. Even though the net energy barriers for the minimum energy pathways for both systems are similar, a concerted direct process in P(EO-MO) allows for easier transport from one cage to another as compared to the stepwise process in PEO. We also observe that for a Li ion to transition from a fully polymer oxygen coordinated state to one with at least one oxygen from the TFSI anion has much higher thermal activation energies on average in P(EO-MO) as compared to PEO, which would further elucidate why there is a much lower ion-pair concentration in P(EO-MO).

Understanding Li-Polymer Connectivity. In the previous section, we observed that the transport mechanism for the most efficacious[37] of the MO-containing polymers, P(EO-MO), is probably more efficient at the same effective temperature. Unfortunately, even though the neat polymers
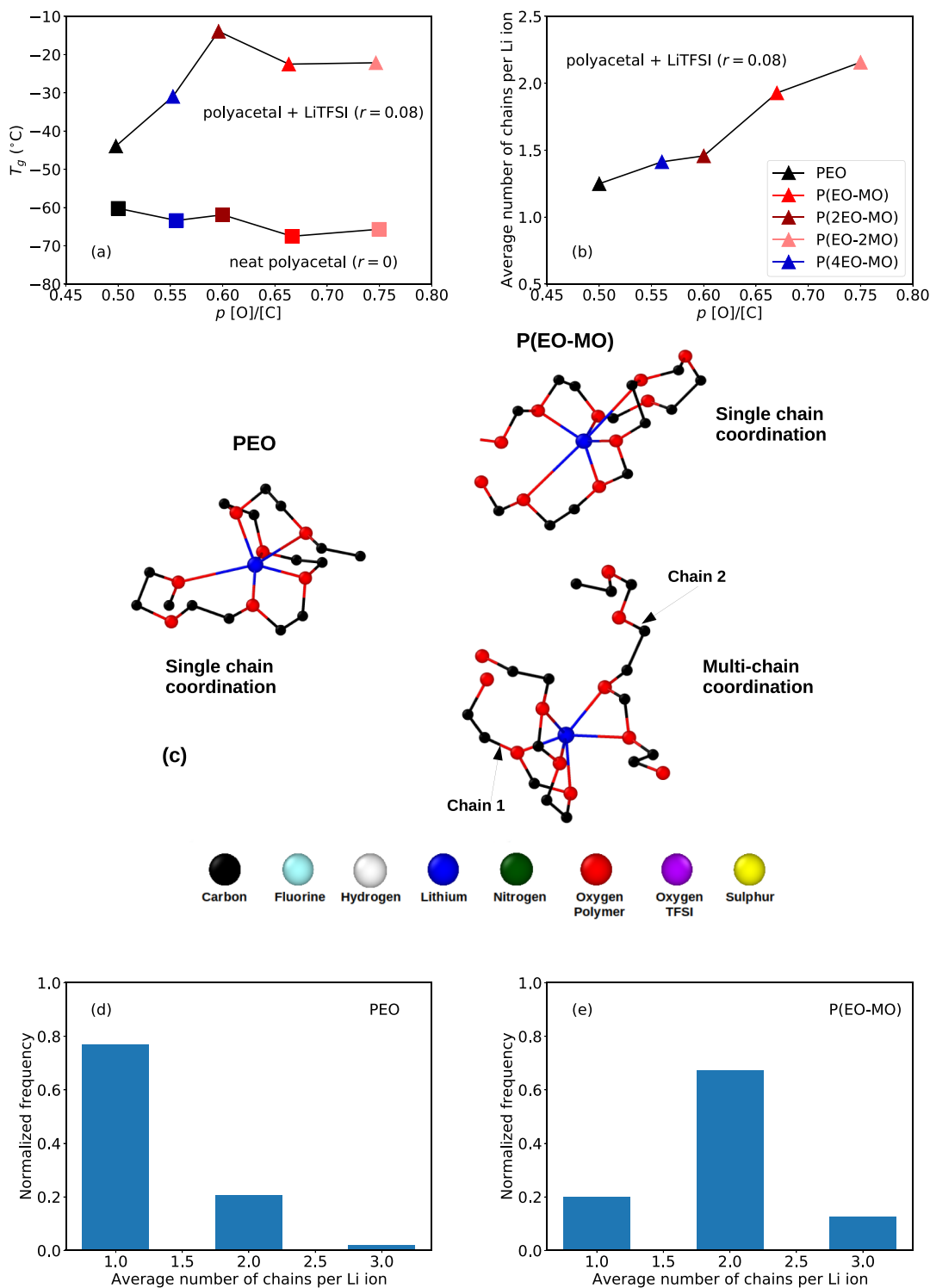
Figure 7. (a) Effect of salt loading on glass-transition temperatures from experiments.[36] (b) Average number of chains for different polymers required to coordinate a Li ion. (c) Representative snapshot of single-chain coordination of a Li atom observed in our simulations in PEO and both single-chain and multi-chain coordination in P(EO-MO). (d) Normalized frequency of finding a Li ion coordinated by different numbers of chains for PEO and (e) P(EO-MO) at 363 K.

have similar glass-transition temperatures, it was observed in our previous work[36] that addition of salt to the MO-containing polymers results in a larger increase in glass-transition temperature as compared to PEO, as seen in the left panel of Figure 7a.

This increase in the glass-transition temperature can be directly correlated with the number of polymer chains involved in coordinating Li ions (see Figure 7b). It is observed that in the MO-containing polymers, multiple chains are involved in coordinating individual Li ions. A single chain of PEO on the other hand is more easily able to provide all the required oxygen atoms to fully coordinate the Li ion. Figure 7c shows representative snapshots of 6-fold coordinated Li ions in PEO coordinated by a single chain and in P(EO-MO) coordinated

by a single chain and two chains. We observe from a 50 ns simulation in the *NVT* ensemble at 363 K that in PEO, a Li ion on average is 80% coordinated by a single chain but only about 20% by two chains, with a negligible amount of three-chain coordination (see Figure 7d). On the other hand, in P(EO-MO), two-chain coordination predominates (70%), with single-chain and three-chain coordination being comparable to each other at about 15% (see Figure 7d).

We can speculate from the above data that in PEO, ion transport along polymer chains is much more common, with two-chain coordination occurring when the ion hops from one chain to another. In contrast, in P(EO-MO), Li-ion hopping between polymer chains occurs more frequently due to an inability to move along a single chain or that fully coordinated states are more energetically favorable when they involve two polymer chains. If the former is true, then P(EO-MO) facilitates a more three-dimensional ion transport mechanism, as compared to quasi-1D transport along single chains in PEO. Either way, the binding of multiple chains by the Li ions results in an undesirable increase in the T_g. The direct consequence of this is that in the polymers we have studied, even though the transport mechanism is possibly more efficient in the MO-containing polyacetals, their higher glass-transition temperature leads to lower performance at battery working temperatures with respect to PEO. Free-energy calculations to elucidate the relative stabilities of the binding motifs in these polymers and the energetics of moving along chains and between chains are currently ongoing, with the aim to help design new polymer electrolytes with favorable glass-transition temperatures and transport mechanisms.

CONCLUSIONS

In this work, we predominantly study two systems from the series of polymer electrolytes studied in our previous work,[36,37] PEO and P(EO-MO) with LiTFSI, to gain insight into local ion coordination environments. Advanced free-energy sampling methods show the existence of multiple distinct coordination environments and their relative stabilities. The ordering of the associated populations of the coordinations is consistent with standard MD sampling; however, we view the MD-sampled populations as overestimates. We observe that the P(EO-MO) electrolyte on the whole prefers ion coordination environments with higher CNs as compared to PEO and has much more diffuse coordination environments. Furthermore, PEO has a less efficient, stepwise free-energy minimum pathway for interconversion of coordination states that involves sequentially forming and breaking bonds, while P(EO-MO) has a more direct path between coordination environments and achieves this in a more concerted and efficient way. However, performant electrolytes for battery materials require efficient mechanisms of transport coupled with low glass-transition temperatures. Even with a possibly less efficient transport mechanism at a given effective temperature, PEO still has a lower glass-transition temperature at specific salt loading and hence is still the most suited in this series of polymers for electrolyte materials for battery applications. We observe that a possible reason for this is single-chain coordination in PEO as compared to a higher propensity for multi-chain coordination in polyacetal systems. Further research to understand the energetics of these different binding motifs and transport along and between chains is currently ongoing to understand the correlation between the local structure and macroscopic properties to guide future design of polymers that can compete with PEO electrolytes.

ASSOCIATED CONTENT

Supporting Information

The Supporting Information is available free of charge at https://pubs.acs.org/doi/10.1021/acs.macromol.1c01417.

Details of the parameters used in the MD simulations for the LJ, bond, angle, and dihedral interactions for the potential used; details on the modi_cations to LJ parameters of the terminal carbons for fixing the density of shorter-chain-length polymers for future work along with the comparison of densities predicted by these potentials for oligomers of di_erent lengths; details of the parameters used in the metadynamics simulations; starting configurations for initial tests; and comparison of these preliminary simulations (PDF)

AUTHOR INFORMATION

Corresponding Author

Siddharth Sundararaman − *Joint Center for Energy Storage Research, the Molecular Foundry, Lawrence Berkeley National Laboratory, Berkeley, California 94720, United States;* orcid.org/0000-0002-4746-879X;
Email: ssundararaman@lbl.gov

Authors

David M. Halat − *Joint Center for Energy Storage Research, Department of Chemical and Biomolecular Engineering and College of Chemistry, University of California Berkeley, Berkeley, California 94720, United States; Joint Center for Energy Storage Research, Materials Sciences Division, Lawrence Berkeley National Laboratory, Berkeley, California 94720, United States;* orcid.org/0000-0002-0919-1689

Youngwoo Choo − *Joint Center for Energy Storage Research, Materials Sciences Division, Lawrence Berkeley National Laboratory, Berkeley, California 94720, United States;* orcid.org/0000-0003-2715-0618

Rachel L. Snyder − *Joint Center for Energy Storage Research, Department of Chemistry and Chemical Biology, Baker Laboratory, Cornell University, Ithaca, New York 14853, United States;* orcid.org/0000-0002-0569-0704

Brooks A. Abel − *Joint Center for Energy Storage Research, Department of Chemistry and Chemical Biology, Baker Laboratory, Cornell University, Ithaca, New York 14853, United States;* orcid.org/0000-0002-2288-1975

Geoffrey W. Coates − *Joint Center for Energy Storage Research, Department of Chemistry and Chemical Biology, Baker Laboratory, Cornell University, Ithaca, New York 14853, United States;* orcid.org/0000-0002-3400-2552

Jeffrey A. Reimer − *Joint Center for Energy Storage Research, Department of Chemical and Biomolecular Engineering and College of Chemistry, University of California Berkeley, Berkeley, California 94720, United States; Joint Center for Energy Storage Research, Materials Sciences Division, Lawrence Berkeley National Laboratory, Berkeley, California 94720, United States;* orcid.org/0000-0002-4191-3725

Nitash P. Balsara − *Joint Center for Energy Storage Research, Department of Chemical and Biomolecular Engineering and College of Chemistry, University of California Berkeley, Berkeley, California 94720, United States; Joint Center for Energy Storage Research, Materials Sciences Division,*

Lawrence Berkeley National Laboratory, Berkeley, California
94720, United States; ⊙ orcid.org/0000-0002-0106-5565

David Prendergast − *Joint Center for Energy Storage*
Research, the Molecular Foundry, Lawrence Berkeley
National Laboratory, Berkeley, California 94720, United
States; ⊙ orcid.org/0000-0003-0598-1453

Complete contact information is available at:
https://pubs.acs.org/10.1021/acs.macromol.1c01417

Notes

The authors declare no competing financial interest.

■ REFERENCES

(1) Whittingham, M. S. Lithium batteries and cathode materials. *Chem. Rev.* **2004**, *104*, 4271−4302.

(2) Lu, L.; Han, X.; Li, J.; Hua, J.; Ouyang, M. A review on the key issues for lithium-ion battery management in electric vehicles. *J. Power Sources* **2013**, *226*, 272−288.

(3) Xu, K. Nonaqueous liquid electrolytes for lithium-based rechargeable batteries. *Chem. Rev.* **2004**, *104*, 4303−4418.

(4) Tarascon, J.-M.; Armand, M. Issues and challenges facing rechargeable lithium batteries. *Nature* **2010**, 171−179.

(5) Wong, D. H. C.; Thelen, J. L.; Fu, Y.; Devaux, D.; Pandya, A. A.; Battaglia, V. S.; Balsara, N. P.; DeSimone, J. M. Nonflammable perfluoropolyether-based electrolytes for lithium batteries. *Proc. Natl. Acad. Sci. U.S.A.* **2014**, *111*, 3327−3331.

(6) Xue, Z.; He, D.; Xie, X. Poly (ethylene oxide)-based electrolytes for lithium-ion batteries. *J. Mater. Chem. A* **2015**, *3*, 19218−19253.

(7) Diddens, D.; Heuer, A. Simulation study of the lithium ion transport mechanism in ternary polymer electrolytes: the critical role of the segmental mobility. *J. Phys. Chem. B* **2014**, *118*, 1113−1125.

(8) Armand, M.; Tarascon, J.-M. Building better batteries. *nature* **2008**, *451*, 652−657.

(9) Christie, A. M.; Lilley, S. J.; Staunton, E.; Andreev, Y. G.; Bruce, P. G. Increasing the conductivity of crystalline polymer electrolytes. *Nature* **2005**, *433*, 50−53.

(10) Fenton, D. E.; Parker, J. M.; Wright, P. V. Complexes of alkali metal ions with poly (ethylene oxide). *Polymer* **1973**, *14*, 589.

(11) Wright, P. V. Electrical conductivity in ionic complexes of poly (ethylene oxide). *Br. Polym. J.* **1975**, *7*, 319−327.

(12) Armand, M. Polymer solid electrolytes-an overview. *Solid State Ionics* **1983**, *9−10*, 745−754.

(13) Mindemark, J.; Lacey, M. J.; Bowden, T.; Brandell, D. Beyond PEO—Alternative host materials for Li+-conducting solid polymer electrolytes. *Prog. Polym. Sci.* **2018**, *81*, 114−143.

(14) Meyer, W. H. Polymer electrolytes for lithium-ion batteries. *Adv. Mater.* **1998**, *10*, 439−448.

(15) Di Noto, V.; Lavina, S.; Giffin, G. A.; Negro, E.; Scrosati, B. Polymer electrolytes: Present, past and future. *Electrochim. Acta* **2011**, *57*, 4−13.

(16) Manuel Stephan, A.; Nahm, K. S. Review on composite polymer electrolytes for lithium batteries. *Polymer* **2006**, *47*, 5952−5964.

(17) Quartarone, E.; Mustarelli, P.; Magistris, A. PEO-based composite polymer electrolytes. *Solid State Ionics* **1998**, *110*, 1−14.

(18) Xu, K. Electrolytes and interphases in Li-ion batteries and beyond. *Chem. Rev.* **2014**, *114*, 11503−11618.

(19) Müller-Plathe, F.; van Gunsteren, W. F. Computer simulation of a polymer electrolyte: Lithium iodide in amorphous poly (ethylene oxide). *J. Chem. Phys.* **1995**, *103*, 4745−4756.

(20) Borodin, O.; Smith, G. D. Molecular dynamics simulations of poly (ethylene oxide)/LiI melts. 2. Dynamic properties. *Macromolecules* **2000**, *33*, 2273−2283.

(21) Borodin, O.; Smith, G. D. Mechanism of ion transport in amorphous poly (ethylene oxide)/LiTFSI from molecular dynamics simulations. *Macromolecules* **2006**, *39*, 1620−1629.

(22) Diddens, D.; Heuer, A. Lithium ion transport mechanism in ternary polymer electrolyte-ionic liquid mixtures: A molecular dynamics simulation study. *ACS Macro Lett.* **2013**, *2*, 322−326.

(23) Do, C.; Lunkenheimer, P.; Diddens, D.; Götz, M.; Weiss, M.; Loidl, A.; Sun, X. G.; Allgaier, J.; Ohl, M. Li+ transport in poly (ethylene oxide) based electrolytes: neutron scattering, dielectric spectroscopy, and molecular dynamics simulations. *Phys. Rev. Lett.* **2013**, *111*, 018301.

(24) Molinari, N.; Mailoa, J. P.; Kozinsky, B. Effect of salt concentration on ion clustering and transport in polymer solid electrolytes: a molecular dynamics study of peo−litfsi. *Chem. Mater.* **2018**, *30*, 6298−6306.

(25) Merinov, B. V.; et al. Molecular Dynamics Simulations of Ionic Diffusion in PEO-LiTFSI Polymer Electrolyte: Effect of Temperature, Molecular Weight, and Ionic Concentration. *ECS Meet. Abstr.* **2018**, DOI: 10.1149/ma2018-02/6/467.

(26) Gartner, T. E., III; Jayaraman, A. Modeling and simulations of polymers: a roadmap. *Macromolecules* **2019**, *52*, 755−786.

(27) Gudla, H.; Zhang, C.; Brandell, D. Effects of solvent polarity on Li-ion diffusion in polymer electrolytes: An all-atom molecular dynamics study with charge scaling. *J. Phys. Chem. B* **2020**, *124*, 8124−8131.

(28) Brooks, D. J.; Merinov, B. V.; Goddard, W. A., III; Kozinsky, B.; Mailoa, J. Atomistic description of ionic diffusion in PEO−LiTFSI: Effect of temperature, molecular weight, and ionic concentration. *Macromolecules* **2018**, *51*, 8987−8995.

(29) Joost, M.; Kunze, M.; Jeong, S.; Schönhoff, M.; Winter, M.; Passerini, S. Ionic mobility in ternary polymer electrolytes for lithium-ion batteries. *Electrochim. Acta* **2012**, *86*, 330−338.

(30) Baskin, A.; Prendergast, D. "Ion Solvation Spectra": Free Energy Analysis of Solvation Structures of Multivalent Cations in Aprotic Solvents. *J. Phys. Chem. Lett.* **2019**, *10*, 4920−4928.

(31) Baskin, A.; Prendergast, D. Ion Solvation Engineering: How to Manipulate the Multiplicity of the Coordination Environment of Multivalent Ions. *J. Phys. Chem. Lett.* **2020**, *11*, 9336−9343.

(32) Kästner, J. Umbrella sampling. *Wiley Interdiscip. Rev.: Comput. Mol. Sci.* **2011**, *1*, 932−942.

(33) Ferguson, A. L. BayesWHAM: A Bayesian approach for free energy estimation, reweighting, and uncertainty quantification in the weighted histogram analysis method. *J. Comput. Chem.* **2017**, *38*, 1583−1605.

(34) Laio, A.; Gervasio, F. L. Metadynamics: a method to simulate rare events and reconstruct the free energy in biophysics, chemistry and material science. *Rep. Prog. Phys.* **2008**, *71*, 126601.

(35) Barducci, A.; Bonomi, M.; Parrinello, M. Metadynamics. *Wiley Interdiscip. Rev.: Comput. Mol. Sci.* **2011**, *1*, 826−843.

(36) Halat, D. M.; Snyder, R. L.; Sundararaman, S.; Choo, Y.; Gao, K. W.; Hoffman, Z. J.; Abel, B. A.; Grundy, L. S.; Galluzzo, M. D.; Gordon, M. P.; et al. Modifying Li+ and Anion Diffusivities in Polyacetal Electrolytes: A Pulsed-Field-Gradient NMR Study of Ion Self-Diffusion. *Chem. Mater.* **2021**, *33*, 4915−4926.

(37) Snyder, R. L.; Choo, Y.; Gao, K. W.; Halat, D. M.; Abel, B. A.; Sundararaman, S.; Prendergast, D.; Reimer, J. A.; Balsara, N. P.; Coates, G. W. Improved Li+ Transport in Polyacetal Electrolytes: Conductivity and Current Fraction in a Series of Polymers. *ACS Energy Lett.* **2021**, *6*, 1886−1891.

(38) Wang, J.; Wolf, R. M.; Caldwell, J. W.; Kollman, P. A.; Case, D. A. Development and testing of a general amber force field. *J. Comput. Chem.* **2004**, *25*, 1157−1174.

(39) Plimpton, S. Fast parallel algorithms for short-range molecular dynamics. *J. Comput. Phys.* **1995**, *117*, 1−19.

(40) Bayly, C. I.; Cieplak, P.; Cornell, W.; Kollman, P. A. A well-behaved electrostatic potential based method using charge restraints for deriving atomic charges: the RESP model. *J. Phys. Chem.* **1993**, *97*, 10269−10280.

(41) Ufimtsev, I. S.; Martínez, T. J. Quantum chemistry on graphical processing units. 1. Strategies for two-electron integral evaluation. *J. Chem. Theory Comput.* **2008**, *4*, 222−231.

(42) Ufimtsev, I. S.; Martinez, T. J. Quantum chemistry on graphical processing units. 2. Direct self-consistent-field implementation. *J. Chem. Theory Comput.* **2009**, *5*, 1004−1015.

(43) Ufimtsev, I. S.; Martinez, T. J. Quantum chemistry on graphical processing units. 3. Analytical energy gradients, geometry optimization, and first principles molecular dynamics. *J. Chem. Theory Comput.* **2009**, *5*, 2619−2628.

(44) Zhang, Y.; Maginn, E. J. A simple AIMD approach to derive atomic charges for condensed phase simulation of ionic liquids. *J. Phys. Chem. B* **2012**, *116*, 10036−10048.

(45) Youngs, T. G. A.; Hardacre, C. Application of static charge transfer within an ionic-liquid force field and its effect on structure and dynamics. *ChemPhysChem* **2008**, *9*, 1548−1558.

(46) Pesko, D. M.; Timachova, K.; Bhattacharya, R.; Smith, M. C.; Villaluenga, I.; Newman, J.; Balsara, N. P. Negative transference numbers in poly (ethylene oxide)-based electrolytes. *J. Electrochem. Soc.* **2017**, *164*, No. E3569.

(47) Iannuzzi, M.; Laio, A.; Parrinello, M. Efficient exploration of reactive potential energy surfaces using Car-Parrinello molecular dynamics. *Phys. Rev. Lett.* **2003**, *90*, 238302.